JOURNAL OF GEOPHYSICAL RESEARCH, VOL. 114, D08114, doi:10.1029/2008JD010602, 2009

A case study of a mesospheric bore event observed with an all-sky airglow imager at Tirunelveli (8.7°N)

V. Lakshmi Narayanan,[1] S. Gurubaran,[1] and K. Emperumal[1]

Received 13 June 2008; revised 11 January 2009; accepted 16 February 2009; published 25 April 2009.

[1] A prominent front separating bright and dark regions of all-sky airglow images was recorded on the night of 22/23 March 2007, at the low-latitude Indian station Tirunelveli (8.7°N, 77.8°E) and is attributed to a mesospheric bore. With the help of complementary wind information from the colocated MF radar and temperature and density data from the SABER instrument onboard TIMED mission, the parameters of the bore are calculated and discussed. Because the observed wind at the emission altitude was orthogonal to the direction of bore propagation, Doppler ducting was not likely to support the bore. The analysis that makes use of the square of buoyancy frequency profiles reveals a thermal duct that would provide favorable conditions for the propagation of the bore. This is the first report of a mesospheric bore event from the Indian sector.

Citation: Narayanan, V. L., S. Gurubaran, and K. Emperumal (2009), A case study of a mesospheric bore event observed with an all-sky airglow imager at Tirunelveli (8.7°N), *J. Geophys. Res.*, *114*, D08114, doi:10.1029/2008JD010602.

1. Introduction

[2] All-sky airglow imagers are potential tools to monitor the dynamics modulated airglow layers, as they capture the wide-field images of the sky with a fisheye lens and store them digitally with the help of CCD arrays. These imagers are most suited for the study and visualization of short-scale disturbances that often modulate the mesospheric airglow emissions. The imaging observations in the past have led to the classification of dynamical events into different types such as quasimonochromatic gravity waves [e.g., *Taylor et al.*, 1997; *Nakamura et al.*, 1999], ripples [*Hecht*, 2004], mesospheric walls [*Swenson et al.*, 1998; *Li et al.*, 2007] and mesospheric bores [*Taylor et al.*, 1995; *Smith et al.*, 2003; *She et al.*, 2004], based on their morphology and propagation characteristics.

[3] During ALOHA-93, *Taylor et al.* [1995] observed a system of wavefronts phase-locked to a leading front behind which the lower airglow layers of hydroxyl and sodium showed an increase in brightness, while the upper layers of atomic and molecular oxygen showed a decrease. This phase reversal property between lower and upper airglow emissions is known as the "complementarity effect". In addition to this behavior of airglow emission intensities, the rotational temperatures derived from OH Meinel band rotational line intensities showed an abrupt increase about 15 minutes before the passage of the front. In order to explain such distinct events, two models have been proposed: (1) *Munasinghe et al.* [1998] explained this event as a propagation of fully ducted gravity wave with observed wave parameters interacting with a waveguide node present in the region between OH and OI emission altitudes; (2) *Dewan and Picard* [1998] interpreted this event as a mesospheric bore and developed a simple model based on the work on channel bores by *Rayleigh* [1908], *Lighthill* [1979] and others (see the references in *Dewan and Picard* [1998]). According to the latter model, mesospheric bores result from symmetric hydraulic jumps that occur in the duct channels present in the upper mesosphere. This model predicted various properties associated with such events and presented an elegant explanation for the observed complementarity effect by considering a simple duct channel that could be provided by a mesospheric inversion layer.

[4] In a subsequent work, *Dewan and Picard* [2001] suggested the forcing due to gravity wave critical level interactions as a favorable condition for the generation of bore disturbances that could impart further energy to an already existing inversion layer. *Seyler* [2005] discussed the possibility of nonlinear development of gravity waves trapped in an inversion layer being seen as mesospheric bores.

[5] A variety of mesospheric bore events have been reported in the literature [*Smith et al.*, 2003, 2005, 2006; *Brown et al.*, 2004; *She et al.*, 2004; *Fechine et al.*, 2005; *Neilson et al.*, 2006; *Shiokawa et al.*, 2006]. Most of them were from low and mid latitude American sector. According to our knowledge, only one bore-like event was reported from the low latitude Indonesian region [*Shiokawa et al.*, 2006] and one event was reported from Antarctica [*Stockwell et al.*, 2006; *Neilson et al.*, 2006]. It appears that bore occurrences are greater in number at low and mid latitudes than at high latitudes [*Fechine et al.*, 2005; *Neilson et al.*, 2006]. However, unless observations from various longitudinal sectors are made, the global distribution of bore occurrences cannot be studied.

[6] For the first time, we herein report a bore event observed using an all-sky airglow imager from the low

[1]Equatorial Geophysical Research Laboratory, Indian Institute of Geomagnetism, Krishnapuram, Tirunelveli, India.

0148-0227/09/2008JD010602$09.00

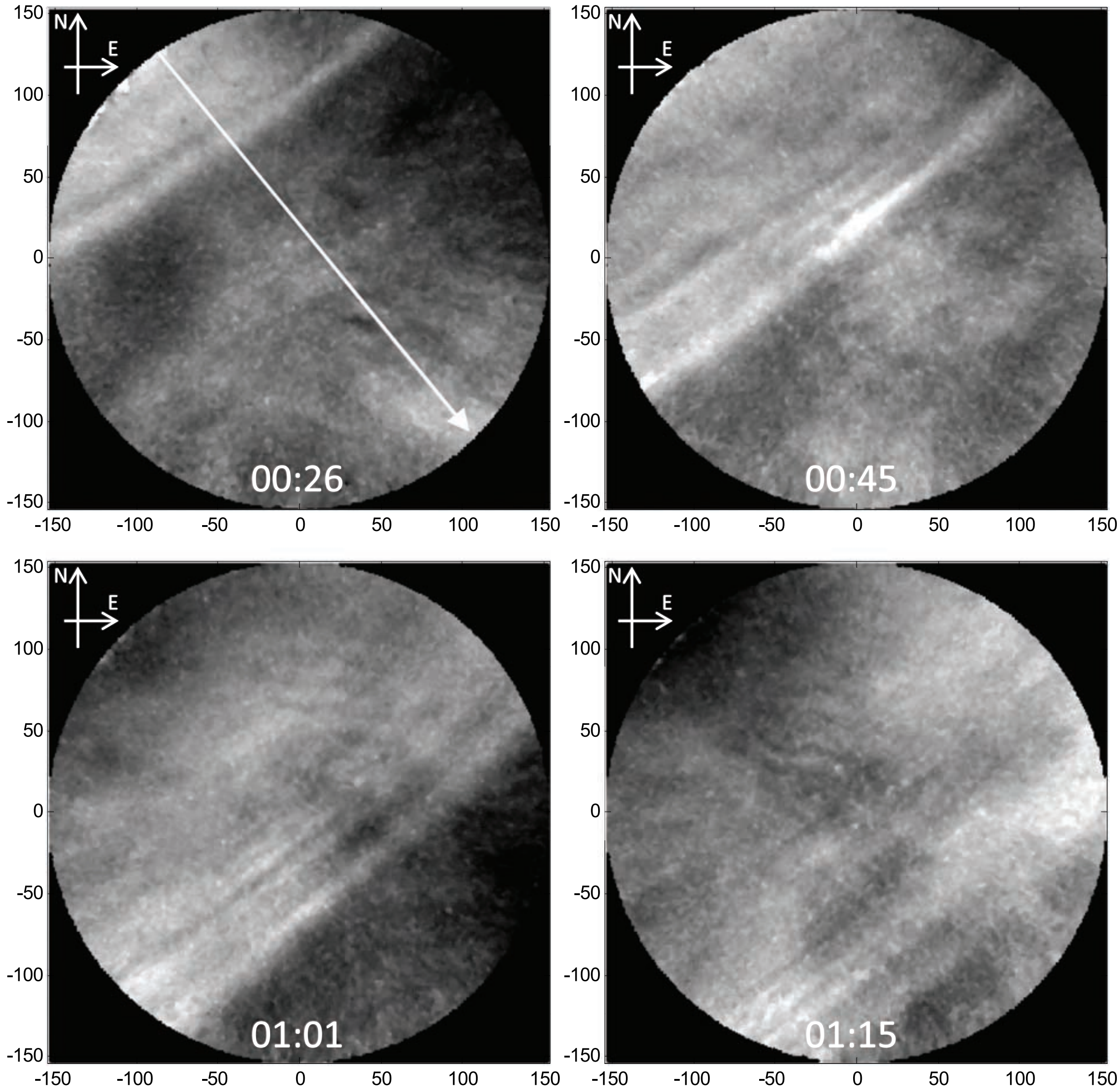

Figure 1. Images showing bore propagation along the direction indicated by the arrow. Times are in IST. The horizontal and vertical axes show distance in kilometers. Assumed height of OH airglow for image unwrapping is 87 km.

latitude Indian site, Tirunelveli (8.7°N, 77.8°E). In this work, with the help of wind data obtained by the colocated medium frequency (MF) radar and temperature data from the Sounding of the Atmosphere using Broadband Emission Radiometry (SABER) instrument onboard Thermosphere Ionosphere Mesosphere Energetics and Dynamics (TIMED) satellite, we infer that the bore was supported by a thermal duct situated at the OH emission altitudes. We explain the observed event in the light of the *Dewan and Picard* [1998] model of mesospheric bores (hereafter referred to as DP model). This model evaluates bore parameters by taking into account the thickness or vertical width of the duct channel before the occurrence of the hydraulic jump denoted by h_0 and the vertical width of the duct channel after the occurrence of the hydraulic jump denoted by h_1. In the present work, the vertical width of the duct channel is simply referred to as duct width. We propose a hypothesis on the possible relationship between the double peaked hydroxyl emission features noticed in SABER observations and the mesospheric bores, albeit further studies and results are awaited for confirmation of this view.

2. Observations and Data Used

[7] Nightglow imaging observations were carried out from Tirunelveli using an all-sky airglow imaging system procured from Keo Scientific Limited, Canada, which is based on f/4 optics with digital image acquisition system consisting of a high efficiency CCD camera of array size 512 × 512 pixels. The instrument is capable of observing the sky from horizon to horizon (>170°). In order to reduce spurious vehicular light disturbance originating in the near-

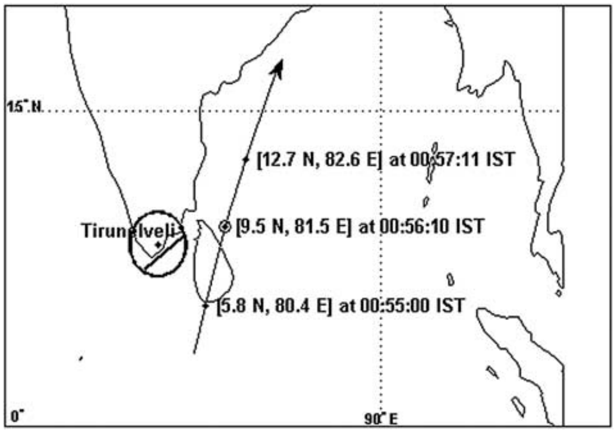

Figure 2. Map showing the ground site of imager observations and the nearby sites over which tangent-point measurements were made by TIMED mission during the progress of the event. The circle around the observation site represents the area covered by the FOV of the imager, and the line inside it is the indication of the leading bore front at 00:56 IST. The parameters sampled by SABER/TIMED over the circled point at geographic coordinates (9.5°N, 81.5°E) is considered to represent the background condition (see text for further details).

by road, we have physically reduced the field of view (FOV) to ~125°. The imager currently hosts the following six filters in a filter wheel arrangement: (1) a broadband OH filter covering the wavelength region of 705.8 to 928.2 nm with a notch centered at 865 nm to block the O_2 band emissions, (2) a filter centered at 557.7 nm to probe the OI green line emission, (3) a sodium filter with a peak transmission wavelength of 589.2 nm, (4) a filter with peak transmission at 572.3 nm to characterize the sky noise, (5) a filter tuned to 630.0 nm and (6) a filter tuned to 777.4 nm. The latter two filters are used to diagnose the thermospheric OI emissions. All the filters except the broadband OH filter have bandwidths less than 2 nm. The acquired images were flat-fielded and the stars present in the images were removed. Thereafter, each of the images that would result by subtracting from it an hourly average of several images was unwarped and projected onto a distance grid. For OH images, the distance grid was based on an assumed centroid height of 87 km. The grid size was approximately 320 × 320 km for 125° FOV, and wave parameters like wavelengths and phase velocities were measured from the unwarped images. This image analysis was similar to that adopted by *Garcia et al.* [1997].

[8] On the night of March 22/23, 2007, an intense system of phase-locked wavefronts moving from northwest to southeast was recorded between 00:25 and 01:30 Indian Standard Time (IST) (IST = UT + 5.5 hours). The horizontal extent of the wavefronts was greater than the distance covered by the FOV of the instrument (~320 km) and they crossed the zenith around 00:50 IST. Figure 1 shows four images of the event obtained at different times during this night. A detailed analysis to be presented in section 3 identifies this event to be a mesospheric bore. On this night, only the OH and background filters were used, with 1 min exposure time for OH images and 2.5 min exposure time for the background images.

[9] In this work, we make use of the wind measurements obtained from the colocated MF radar. The radar is capable of determining wind velocities from 68 to 98 km at a height resolution of ~4 km. The probing region is oversampled at 2 km height intervals. Typical uncertainties of wind estimates are ~5 m/s. Further details of the radar system and the method of wind extraction are outlined by *Rajaram and Gurubaran* [1998] and references therein. Adopting a criterion of at least 30% of useful data obtained every hour, we found the radar probing height region of 84–94 km suitable for analysis.

[10] Along with these ground-based data sets, the temperature, density and 1.6 μm OH emission measurements made by the SABER instrument onboard TIMED satellite are used to calculate the parameters of the bore. During the event, the TIMED mission made tangent point measurements over locations with geographic coordinates (5.8°N, 80.4°E) at 00:55:00 IST, (9.5°N, 81.5°E) at 00:56:10 IST and (12.7°N, 82.6°E) at 00:57:11 IST as shown in Figure 2. The distances between the ground observation station (8.7°N, 77.8°E) and the satellite measurement locations over (5.8°N, 80.4°E), (9.5°N, 81.5°E) and (12.7°N, 82.6°E) are 437.9 km, 422.0 km and 697.7 km, respectively. The measurement nearest to our ground observation site corresponded to the location with geographic coordinates (9.5°N, 81.5°E) and also this measurement was nearer to the observed frontal system as depicted in Figure 2. We assume that the parameters measured over this location did not differ appreciably from those over our ground observation site. Thus the values measured over (9.5°N, 81.5°E) are considered to represent the background conditions and we evaluate the parameters of the bore by making use of those values. By the time of this measurement at 00:56:10 IST, the wave system had already crossed the overhead part of the sky at Tirunelveli. It may be noted that the horizontal extent over which the wavefronts got aligned as seen in the images shown in Figure 1 was greater than 320 km, and hence there was a possibility that the bore would have extended up to the longitudes of SABER measurements. Hence the chosen measurement set at (9.5°N, 81.5°E) was likely to represent the background conditions after the bore passage. Figure 2 shows the bore front observed at 00:56 IST as a straight line within a circle representing the FOV of the instrument. Even though the height profiles of the SABER measurements were sampled approximately at 0.4-km intervals, their vertical resolution was ~2 km. Hence for our discussion, we consider parameters averaged over 2 km in 1 km sliding intervals for the altitude region of interest.

3. Results and Discussion

[11] As mentioned before, an intense wavefront entered the imager FOV from the northwest around 00:25 IST and it continued to travel toward the southeast at an azimuth of 140° with no appreciable rotation during the course of the event. The region of images behind the leading front showed enhanced emission intensity. From 00:40 IST onward, at least three crests were seen. The wavelength values shown in Table 1 were deduced for times after 00:40 IST yielding an average horizontal wavelength, λ, of 13.4 km. As time passed

Table 1. Wavelengths Observed Around the Time Specified[a]

Time in IST	C2-C1 (km)	C3-C2 (km)	C4-C3 (km)	C3-C1 (km)
00:45	14.9 ± 1.1	12 ± 1.1	13.3 ± 1.6	27.3 ± 1.5
01:00	13 ± 0.6	12.5 ± 1.2	13.8 ± 1	25.2 ± 1.3
01:15	–	–	14.6 ± 0.9	25 ± 0.6

[a]C1, C2, C3, and C4 represents successive crests from the first one.

by, more fronts became visible, but they were relatively fainter. The second front completely disappeared at around 01:00 IST. Table 1 also lists the computed distance between the first and third fronts at various times. The leading front exited the FOV of the instrument at around 01:25 IST. The apparent phase velocity, c, does not show any significant variation during the course of the observation and is estimated to be 70.0 ± 5.7 m/s. The errors in the estimates correspond to the standard deviations computed for the set of points that contributed to the computation of the wave parameters.

[12] The background wind along the direction of propagation of the frontal system was obtained from the zonal and meridional wind components measured by the MF radar. The average of the 86 and 88 km altitude winds along 140° azimuth obtained between 00:30 and 01:30 IST was 10.3 m/s and is taken as the background wind, u. Thus the intrinsic velocity of phase propagation, U (= $c - u$), of the frontal system is estimated to be 59.7 m/s. The values of λ and c from the imager measurements, u from MF radar measurement and N^2 (square of buoyancy frequency) and H (scale height) calculated from SABER temperature profiles, are substituted in the gravity wave dispersion relation:

$$m^2 = \left(\frac{N^2}{(c-u)^2}\right) - k^2 - \frac{1}{4H^2}, \quad \text{where} \quad k = 2\pi/\lambda. \qquad (1)$$

[13] Here m and k represent the vertical and horizontal wave numbers, respectively. From the above equation, we get an imaginary value for m throughout the height range of 84 to 94 km as shown in Figure 3, which is an indication for evanescence. Any interpretation of this event in terms of a wall wave requires an evidence for the existence of a large-amplitude vertically propagating gravity wave [*Swenson et al.*, 1998; *Batista et al.*, 2002; *Li et al.*, 2007]. In the present work, we do not have evidence for the existence of such a strong vertically propagating wave in the available wind data. Further, the dispersion relation would reveal a propagating feature if the observed wave system was indeed a propagating gravity wave. Rather, the use of the above expression (equation (1)) reveals an evanescent behavior thus defying the identification of the observed event as a wall wave. Furthermore, evanescent waves are not likely to carry enough energy to bring about any increase in the intensity of airglow emissions as witnessed in the present case.

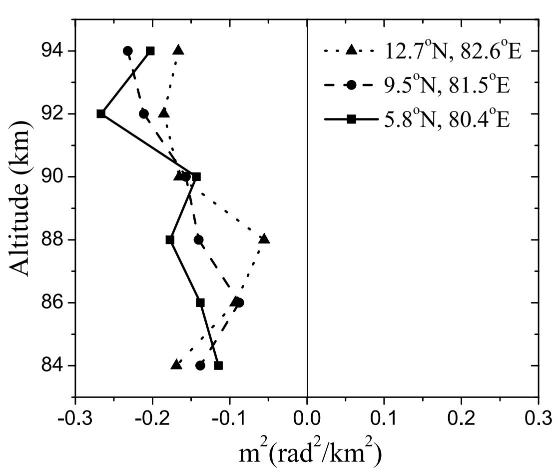

Figure 3. Profile of square of vertical wave number calculated using colocated MF radar winds and N^2 values obtained from temperature measurements over all the three locations.

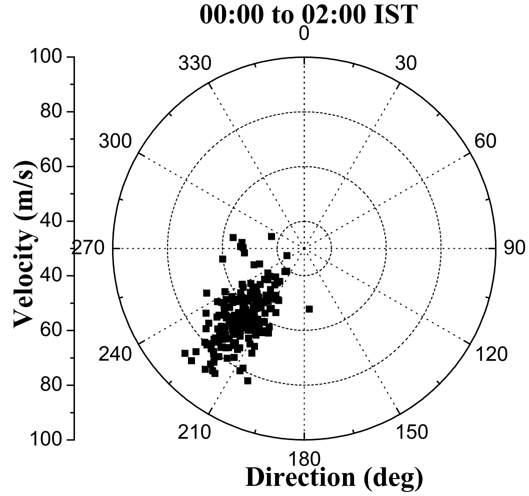

Figure 4. True wind scatterplot for measurements in the height region 86–90 km between 00:00 and 02:00 IST.

[14] A bore can be thought as a kind of discontinuous flow, and the undulations (trailing wavefronts) are believed to be the consequence of energy leakage behind the leading front associated with a hydraulic jump [*Dewan and Picard*, 1998]. They are not merely ducted gravity waves that could be treated with linear theory of gravity waves. Hence it is not necessary for them to satisfy linear dispersion relations of gravity waves. The undulations noted in the very first report of mesospheric bores were indeed evanescent [*Taylor et al.*, 1995; *Isler et al.*, 1997]. A recent work on a bore-like event over Antarctica reported undulations that showed both evanescent as well as freely propagating regions evolving in time [*Neilson et al.*, 2006]. However, some sort of ducting structure is required to support the internal bores. We next examine whether a duct was present during the time of the observed event.

[15] The measured true wind in the vicinity of OH emission altitudes was oriented around 225° azimuth in the 86 to 90 km height region during the time of event as shown in Figure 4. Since the true wind direction was nearly perpendicular to the propagation direction of the observed frontal system, Doppler ducting was unlikely [*Jones*, 1972; *Walterscheid et al.*, 1999]. The two hourly averaged (from 00:00 to 02:00 IST) height profiles of radar winds along the meridional and zonal directions and also along 225° and

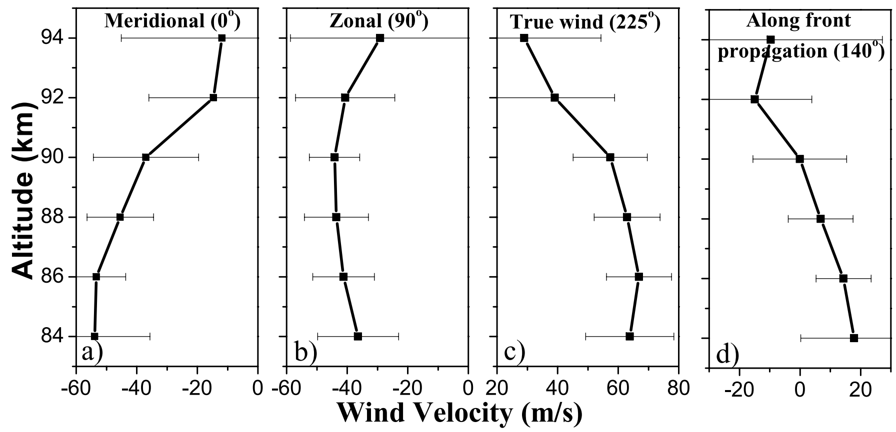

Figure 5. Averaged wind profiles along (a) meridional direction and (b) zonal direction, (c) component along 225° as representative for true wind, and (d) component along the front propagation direction (see text for details). The error bars represent the standard deviations of wind measurements averaged for the 2-hour duration (00:00 IST–02:00 IST).

140° azimuths are shown in Figures 5a–5d, wherein the wind along 225° azimuth refers to the true wind and that along 140° azimuth was the component in the front propagation direction. The error bars in the four columns in Figure 5 represent the standard deviations of wind measurements averaged over the 2-hour period. No Doppler duct structure is evident in the altitude region of 84–94 km in the propagation direction of the bore front (Figure 5d). Nor any intense vertical shear is seen either.

[16] It may be noticed from Figure 5 that the true wind speed at 86 km was ~60 m/s which was as high as the intrinsic bore speed. The radar measurements clearly reveal smaller wind speeds along the propagation direction of the bore, which is in accordance with the previous reports on mesospheric bores [*Taylor et al.*, 1995; *Smith et al.*, 2003; *She et al.*, 2004].

[17] Since Doppler ducting was not evident, the other possibility was thermal ducting that would be caused by the height variations in the square of buoyancy frequency (N^2). The temperatures measured with the SABER instrument are used to calculate the square of the buoyancy frequency given by

$$N^2 = \frac{g}{T}\left(\nabla T_z + \frac{g}{C_p}\right). \quad (2)$$

The acceleration due to gravity, g, is taken as 9.54 ms^{-1} in the above equation with a specific heat C_p = 1005 J Kg^{-1} K^{-1}. ∇T_z is the vertical temperature gradient.

[18] Figure 6 shows the height profiles of N^2 values computed from the temperature measurements. A thermal duct encompassing the OH emission altitudes is indeed seen in the N^2 profiles over the locations (9.5°N, 81.5°E) and (12.7°N, 82.6°E) and the presence of this feature thus supports the identification of the observed event to be a bore event as it would favor the propagation of the bore. The ducts are indicated by dotted lines in Figures 6b and 6c. Noteworthy is the fact that the duct structure is not seen in the N^2 profile over the location (5.8°N, 80.4°E; Figure 6a), which was ahead of the bore front, while the other two locations were behind the bore front (see Figure 2). It may be noted that there is a point of inflection at the region of interest in Figure 6a. It is unclear whether the inflection would have developed into a duct prior to the passage of the bore front over that location at (5.8°N, 80.4°E) in not less than 100 minutes if the front traversed at the intrinsic phase speed of ~60 m/s, or whether the bore front would damp and dissipate owing to the lack of a supporting duct channel. According to our knowledge, the DP model does not discuss the ways of bore dissipation in detail, apart from the fact that energy is lost by means of generation of trailing wavefronts. However, it may be noted that we have utilized the data from only Figure 6b to calculate the bore parameters, where there was a duct.

[19] As mentioned earlier, we calculate the parameters of the bore with the help of the temperature and density measurements made over the location (9.5°N, 81.5°E) by considering them to represent the background condition after the passage of the bore. The half width of the duct highlighted in Figure 6b was 2.5 km and it represents the width h_1 (i.e. the increased duct width after the passage of the bore). In order to calculate the parameters of the bore from the equations of DP model, we need to have information on the duct width (h_0) prior to the passage of the bore.

[20] According to the DP model, the nature of the bore is determined by the bore strength, β, which is defined as the ratio of the increase in duct width to the duct width before the occurrence of hydraulic jump:

$$\beta = \frac{h_1 - h_0}{h_0}. \quad (3)$$

[21] For channel bores, if $\beta < 0.3$, the energy of the bore will be dissipated by the generation of waves behind the front, and such bores are called undular bores. If $\beta > 0.3$, the amplitudes of the waves generated by energy dissipation will be too large to sustain the waves, resulting in wave breaking that leads to turbulence. Such bores are called turbulent or foaming bores. However, for internal bores, this transition criterion (β = 0.3) may not hold rigorously, as

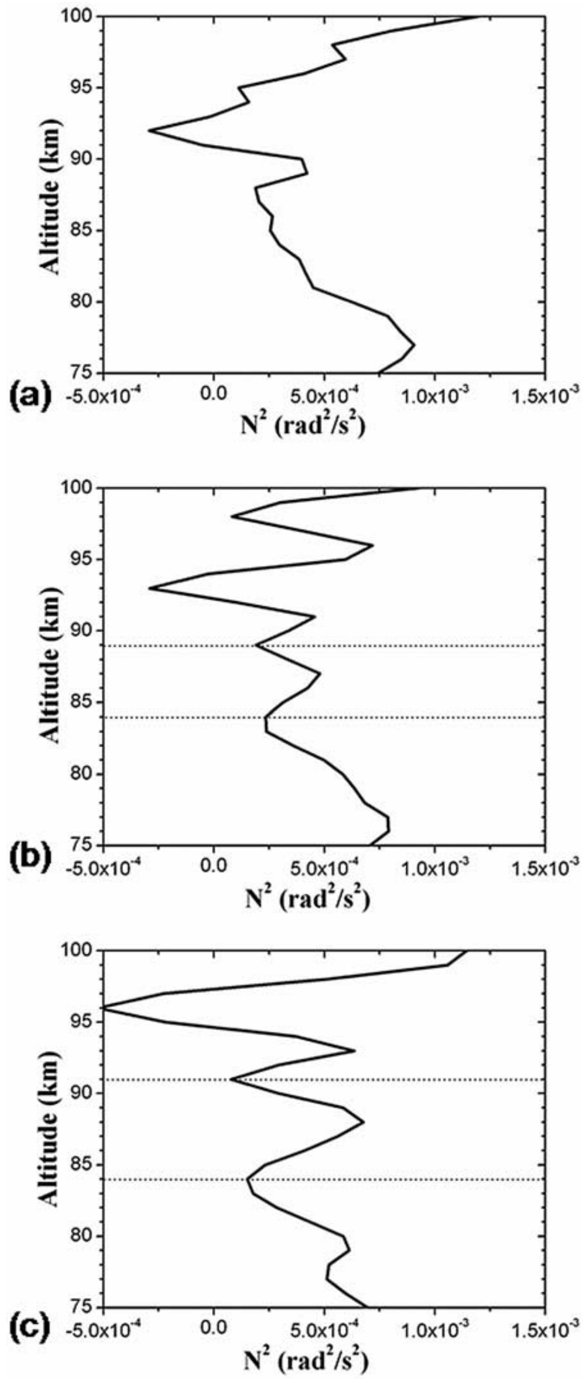

Figure 6. Height profiles of square of buoyancy frequency (N^2) at locations (a) 5.8°N, 80.4°E; (b) 9.5°N, 81.5°E; and (c) 12.7°N, 82.6°E derived from SABER observations.

there is always a possibility of other means of energy dissipation apart from wave generation, like energy leakage through ducts. Indeed, with the help of laboratory experiments on two-layer fluids, *Rottman and Simpson* [1989] found the internal bores are undulatory up to $\beta = 1$, undulations existed with shear instability and mixing for $1 < \beta < 3$ and the internal bores were turbulent for β values greater than 3.

[22] We obtain the bore strength, β, from h_1 and λ using the following equation,

$$\beta = \left(\frac{2\sqrt{2}\pi h_1}{3\lambda}\right)^2. \quad (4)$$

[23] We get the value of β as 0.3, which indicates undulatory nature of the bore as seen in the images (see Figure 1), and no transition to turbulence is seen in our observations.

[24] From this value of β and h_1, we estimate h_0 to be 1.9 km using equation (3). The amplitude of the bore is estimated as 0.46 km from equation (5) [*Dewan and Picard*, 1998] given below

$$a = \frac{h_1 \beta}{\sqrt{3}}. \quad (5)$$

[25] The parameter, a, represents the amplitude of the undulations in the bore, which are indeed superimposed on the existing hydraulic jump. Since the bores recorded in the images are already accompanied by increase or decrease in the emission intensities owing to the hydraulic jumps, separating the contribution of bore amplitudes to the observed undulations is highly challenging.

[26] The phase velocity of the bore (U) according to the DP model is given by

$$U = \sqrt{\frac{g' h_1 (h_1 + h_0)}{2h_0}}, \quad (6)$$

where the parameter g' replaces acceleration due to gravity (g) in channel bore equations and is known as the buoyancy corrected acceleration due to gravity that can be obtained from the ratio of difference in potential temperature across the bore ($\Delta\phi$) and mean potential temperature (ϕ_{avg}):

$$g' = g\left|\frac{\Delta\phi}{\phi_{avg}}\right|, \quad \text{where} \quad \phi = T\left(\frac{P_0}{P}\right)^{0.288}.$$

Here P is the pressure with P_0 being the reference pressure of 1000 mb. The buoyant acceleration due to gravity g' is calculated from the density and temperature profiles obtained by the SABER instrument after the bore passage. We have utilized ideal gas law ($P = \rho RT$, with R = 287.05 J kg^{-1} K^{-1}) to get the pressure from mass density. The number density values obtained from the SABER measurements are converted to mass density values before substituting them in the ideal gas law.

[27] While developing the simplified model of mesospheric bores, *Dewan and Picard* [1998] assumed that the evolution of the bore is symmetrical from a midplane, and hence, they appear like mirror images of each other. However, in reality the values of g' may be different in the upper and lower parts of the duct. Here we evaluate g' and U separately for the upper and lower parts of the thermal duct and obtain values of 0.93 m/s^2 and 0.88 m/s^2, respectively. Corresponding phase velocity values for the

Table 2. Observed and Estimated Parameters of the Bore

Parameters	Observed	Model-Derived Parameters Based on Observed Values	Parameters Obtained From a Sample Calculation
h_0 (km)	–	1.9	2.1[a]
h_1 (km)	2.5	2.5[b]	3.0[a]
β	–	0.30	0.43
λ (km)	13.4	13.4[b]	13.6
a (km)	–	0.46	0.74
n_c	–	5.32	4.92
$U = c - u$ (m/s)[c]	59.7	51.9 (upper), 50.5 (lower)	57.3
dW/dt (waves/hour)	4–5	3.3	3.6

[a]Arbitrarily assumed values from which a sample calculation was carried out whose results are shown in the last column.
[b]The values retained from observations for calculating the bore parameters.
[c]For U, the calculations are made for the channels above and below the duct centroid separately and are referred to as "upper" and "lower", respectively.

upper and lower parts are 51.9 m/s and 50.5 m/s, respectively.

[28] According to the DP model, the measure of nonlinearity of the bore can be inferred from the following parameter, n_c,

$$n_c = a\lambda^2/h_1^3. \quad (7)$$

[29] This parameter is expected to be negligibly small when the undulations are perfectly sinusoidal, and will be approximately around 16 for solitary undulations. For intermediate values, the undulations are likely to be cnoidal in nature. Cnoidal waves are a type of nonlinear waves for which the distance between the crests will increase as time passes and also the distances between the successive crests behind the leading front will be in decreasing order along with their amplitudes [*Drazin and Johnson*, 1989]. The main reason for this nonlinear behavior is the dependence of the phase velocity on the amplitude of the wave crests. For values of n_c well above 16, the bore will be turbulent [*Smith et al.*, 2003]. For our case, the estimated n_c value is 5.32. Because of our reduced field of view, this bore was observed only for about one hour and no regular order in the distances between the successive crests was found (see Table 1). Hence our observations did not reveal any undulations that are cnoidal in nature. For unknown reasons, the amplitude of the second front decreased soon and the front was invisible after 01:00 IST resulting in a broader trough between the first and third crests.

[30] *Dewan and Picard* [1998] also derived the following expression for the number of wave crests that would be generated with time, based on the assumption that the energy was dissipated only by means of trailing wavefronts

$$\frac{dW}{dt} = \frac{U(h_1 - h_0)^3}{2a^2\lambda h_1}. \quad (8)$$

[31] The calculation for our case shows that 3.3 waves can be produced in an hour. This prediction is not easy to test in the case of mesospheric bores, as they are inferred from the airglow emissions. This is because in the case of channel bores newly forming crests are viewed directly in the medium in which they are forming, whereas in mesospheric bores observed through airglow, a newly formed crest will be visible only if it is strong enough to perturb the emitting species in a coherent manner. Also, the energy of the bore gets lessened as more crests are generated. So there is a possibility for the existence of less energetic crests that cannot be visualized in airglow observations. In our case, after about one hour of observations, an addition of approximately four to five crests was seen, though they were not very clear.

[32] A sample calculation, with h_1 = 3 km and h_0 = 2.1 km, reveals a fair match between the observed wavelength and phase speed parameters and those derived from the model. For easy comparison, we have tabulated the bore parameters, namely, β, a, λ_h, U, n_c and dW/dt, with available data from observations, in Table 2.

[33] From Figures 7b and 7c, one can see a double peaked structure in the SABER measured OH emission profiles. It is known that the usual height structure of the mesospheric airglow emissions resembles a Gaussian. Such unusual double peaked structures were noticed in earlier observations by WINDII/UARS satellite mission. *Melo et al.* [2000] discussed such OH height structures in some detail and concluded that thermal inversion layers or vertically propagating gravity waves or mixing could account for them. We may verify that all these three possibilities proposed for the generation of double peaked structures on hydroxyl nightglow can be related to the phenomenon of mesospheric bores. Inversion layers are needed to bring about thermal ducting that can support a bore, and the gravity wave forcing may be responsible for the generation of a mesospheric bore as discussed by *Dewan and Picard* [2001]. *Smith et al.* [2005] found a convincing evidence for this idea. Since a bore is an outcome of vertical hydraulic jumps, vertical mixing of species is expected while atmospheric layers experience a downward or upward body force. Further work by *Liu and Shepherd* [2006] implied that the double peaked structure in the satellite observations of WINDII/UARS could be ascribed to horizontal wave-like structures with wavelengths greater than 100 km. Bores are indeed horizontal step-like functions, and we may associate the double peaked structures in airglow emission profiles with the mesospheric bores by considering them to arise from the movement of the emission layer due to hydraulic jump. Since the temperature and the airglow intensity are

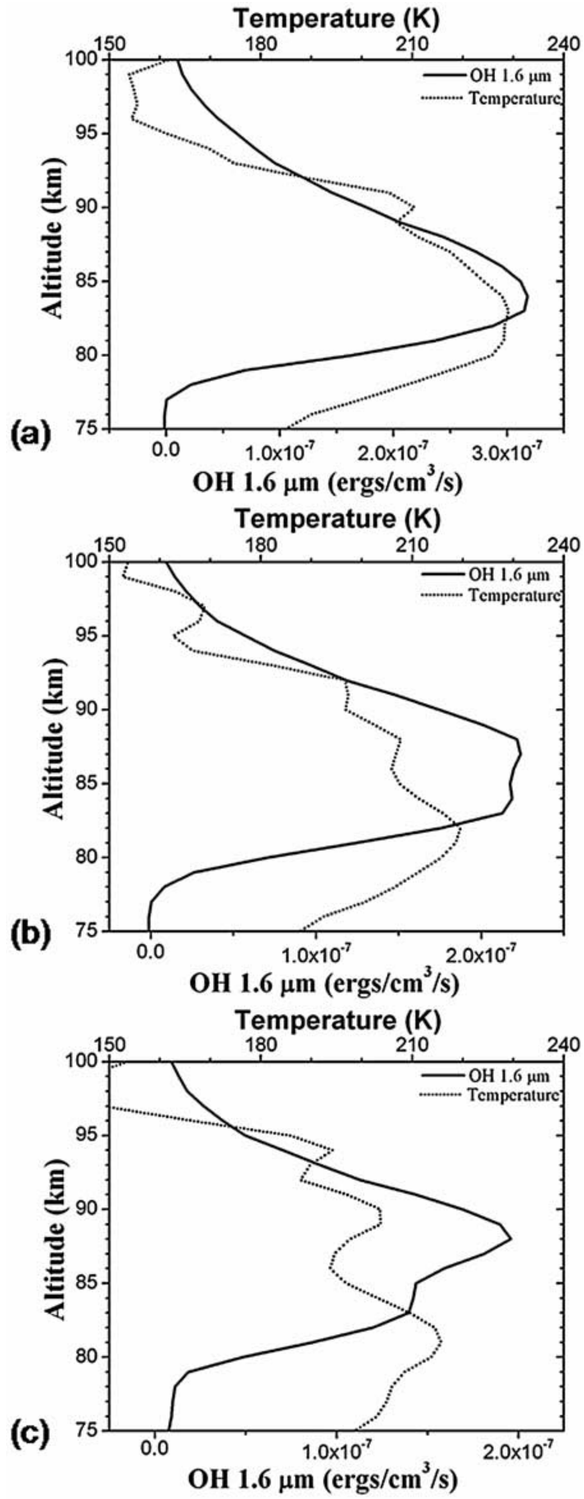

Figure 7. SABER measurements of the height profiles of OH 1.6 μm emission and temperature over the locations (a) 5.8°N, 80.4°E; (b) 9.5°N, 81.5°E; and (c) 12.7°N, 82.6°E.

expected to increase for any downward movement in the upper mesosphere, we may conclude that the emission layer itself might be descending in altitude owing to the intensity rise associated with the bore disturbance noticed in all-sky airglow images.

[34] A bore is mainly a horizontal phase motion of a vertical hydraulic jump and it is not expected to bring about any significant horizontal advection or mixing. So what is expected is the lowering (rising) of the emission layers and the rise (fall) of kinetic temperature of that lowered (raised) emission altitude across the bore. From this insight, we can test one more prediction of DP model that approximates the temperature change across the bore to be $(h_1 - h_0) \times 10$ K. From Figure 7b, assuming that the temperature corresponding to the upper peak of OH emission represents the value before the bore passage and that corresponding to the lower peak of OH emission represents the value after the bore passage, we obtain a difference of ~4.5 K, while the expected difference given by the above formula is 6 K for a bore jump of 0.6 km.

[35] It may be noted that there are wavelike perturbations in the plot of SABER temperatures in Figure 7. The approximate vertical wavelength, λ_z, of these waves is 5 km. In order to examine whether these perturbations were in any way related to the imaging observations of frontal system, we substitute m^2 derived from this value in the dispersion relation (equation (1)). Assuming the same background conditions provided by SABER measurements, the result yields a negative value for k^2 (the square of horizontal wave number). This implies that the wave might not propagate in the horizontal direction, whereas imaging observations revealed horizontal propagation. Moreover, the wave system observed by the imager was found to be evanescent. Above all, those waves with vertical wavelengths less than the thickness of the emission layers (~10 km) would get canceled out in imaging observations. Hence we conclude that the event observed by the imager was not related to the wave-like disturbance noticed in the SABER temperature profiles in Figure 7.

4. Summary

[36] In this work, the intense system of phase-locked crests observed in all-sky airglow imaging observations over Tirunelveli is attributed to a mesospheric bore supporting the model proposed by *Dewan and Picard* [1998, 2001] based on the following characteristics.

[37] 1. There was a front moving with an intrinsic phase velocity of ~60 m/s separating bright and dark regions of images.

[38] 2. There were phase-locked crests that followed the leading front.

[39] 3. A thermal ducting structure was observed at the altitude region of OH emission in which the bore was seen.

[40] 4. An increase in the number of fronts phase-locked to the leading one was seen.

[41] 5. A change in temperature as expected according to the DP model was inferred indirectly.

[42] We do not find evidence for the existence of a large-amplitude vertically propagating gravity wave in the available radar winds to attribute the event to a mesospheric wall wave. Further, this event does not show features of cnoidal waves reported earlier [*Smith et al.*, 2003, 2006]. Since, only OH and background images were recorded on this night, we are unable to discuss about the complementarity

features reported elsewhere [*Taylor et al.*, 1995; *Smith et al.*, 2003; *Brown et al.*, 2004]. The MF radar observations do not reveal the presence of a Doppler duct required to create a bore channel. Rather, the existence of a thermal duct structure was inferred with the help of SABER temperature measurements. A simultaneous double peaked structure was observed in the SABER/TIMED 1.6 μm OH emission measurements and we reasoned it to be an after effect of the bore passage. This idea has not been tested and more observations are required to establish the relationships between double peaked altitude profiles of the airglow emissions and mesospheric bores. However, it seems lowering or rising of the emission layers accompanying the mesospheric bores has the potential to account for at least small-scale and medium-scale double peaked emission profiles noticed in satellite remote sensing observations.

[43] Until now several reports (including this one) identified the background wind speed along the bore propagation direction to be very less compared to the velocity of the bore. This may be an indication for a nearly orthogonal true wind during the passage of a mesospheric bore. In the present case study, the true wind was indeed found to be oriented in a nearly orthogonal direction during the bore propagation.

[44] As mentioned earlier, we have interpreted the event as a mesospheric bore and discussed its characteristics according to the DP model based on a snapshot temperature measurement made by SABER/TIMED satellite mission over a nearby location. However, we feel the analysis might have been more elaborate and conclusive if time series of temperature were available. Coordinated temperature measurements by a sodium lidar will be of immense use and we are hopeful to install a sodium lidar to measure temperatures over our ground observation site in the near future.

[45] **Acknowledgments.** The authors gratefully acknowledge the SABER team and TIMED mission team for providing useful temperature, density, and OH emission data sets. One of the authors (V.L.N.) thanks the Director of Indian Institute of Geomagnetism for a research scholarship. This work is supported by the Department of Science and Technology, Government of India.

References

Batista, P. P., B. R. Clemesha, D. M. Simonich, M. J. Taylor, H. Takahashi, D. Gobbi, I. S. Batista, R. A. Buriti, and A. F. de Medeiros (2002), Simultaneous lidar observation of a sporadic sodium layer, a ‘‘Wall’’ event in the OH and OI5577 airglow images and the meteor winds, *J. Atmos. Sol. Terr. Phys.*, *64*, 1327–1335.

Brown, L. B., A. J. Gerrard, J. W. Meriwether, and J. J. Makela (2004), All-sky imaging observations of mesospheric fronts in OI 557.7 nm and broadband OH airglow emissions: Analysis of frontal structure, atmospheric background conditions, and potential sourcing mechanisms, *J. Geophys. Res.*, *109*, D19104, doi:10.1029/2003JD004223.

Dewan, E. M., and R. H. Picard (1998), Mesospheric bores, *J. Geophys. Res.*, *103*(D6), 6295–6305.

Dewan, E. M., and R. H. Picard (2001), On the origin of mesospheric bores, *J. Geophys. Res.*, *106*(D3), 2921–2927.

Drazin, P. G., and R. S. Johnson (1989), *Solitons: An Introduction*, Cambridge Univ. Press, New York.

Fechine, J. A., F. Medeiros, R. A. Buriti, H. Takahashi, and D. Gobbi (2005), Mesospheric bore events in the equatorial middle atmosphere, *J. Atmos. Sol. Terr. Phys.*, *67*, 1774–1778, doi:10.1016/j.jastp.2005.04.006.

Garcia, F. J., M. J. Taylor, and M. C. Kelly (1997), Two-dimensional spectral analysis of mesospheric airglow image data, *Appl. Opt.*, *36*(29), 7374–7385.

Hecht, J. H. (2004), Instability layers and airglow Imaging, *Rev. Geophys.*, *42*, RG1001, doi:10.1029/2003RG000131.

Isler, J. R., M. J. Taylor, and D. C. Fritts (1997), Observational evidence of wave ducting and evanescence in the mesosphere, *J. Geophys. Res.*, *102*(D22), 26,301–26,313.

Jones, W. L. (1972), Ducting of internal gravity waves on a stable layer with shear, *J. Geophys. Res.*, *77*(21), 3879–3885.

Li, F., G. R. Swenson, A. Z. Liu, M. Taylor, and Y. Zhao (2007), Investigation of a ‘‘wall’’ wave event, *J. Geophys. Res.*, *112*, D04104, doi:10.1029/2006JD007213.

Lighthill, J. (1979), *Waves in Fluids*, Cambridge Univ. Press, New York.

Liu, G., and G. G. Shepherd (2006), Perturbed profiles of oxygen nightglow emissions as observed by WINDII on UARS, *J. Atmos. Sol. Terr. Phys.*, *68*, 1018–1028.

Melo, S. M., R. P. Lowe, and J. P. Russell (2000), Double-peaked hydroxyl airglow profiles observed from WINDII/UARS, *J. Geophys. Res.*, *105*(D10), 12,397–12,403.

Munasinghe, G., H. Hur, T. Y. Huang, A. Bhattachryya, and T. F. Tuan (1998), Application of dispersion formula to long- and short-period gravity waves: Comparisons with ALOHA-93 data and an analytical model, *J. Geophys. Res.*, *103*(D6), 6467–6481.

Nakamura, T., A. Higashikawa, T. Tsuda, and Y. Matsushita (1999), Seasonal variations of gravity wave structures in OH airglow with a CCD imager at Shigaraki, *Earth Planets Space*, *51*, 897–906.

Neilson, K., M. J. Taylor, R. G. Stockwell, and M. J. Jarvis (2006), An unusual mesospheric bore event observed at high latitudes over Antarctica, *Geophys. Res. Lett.*, *33*, L07803, doi:10.1029/2005GL025649.

Rajaram, R., and S. Gurubaran (1998), Seasonal variabilities of low-latitude mesospheric winds, *Ann. Geophys.*, *16*, 197–204.

Rayleigh, L. (1908), Note on tidal bores, *Proc. R. Soc. Lond. A*, *81*, 448–449.

Rottman, J. W., and J. E. Simpson (1989), The formation of internal bores in the atmosphere: A laboratory model, *Q. J. R. Meteorol. Soc.*, *115*, 941–963.

Seyler, C. E. (2005), Internal waves and undular bores in mesospheric inversion layers, *J. Geophys. Res.*, *110*, D09S05, doi:10.1029/2004JD004685.

She, C. Y., T. Li, B. P. Williams, T. Yuan, and R. H. Picard (2004), Concurrent OH imager and sodium temperature/wind lidar observation of a mesopause region undular bore event over Fort Collins/Plateville, Colorado, *J. Geophys. Res.*, *109*, D22107, doi:10.1029/2004JD004742.

Shiokawa, K., S. Suzuki, Y. Otsuka, T. Ogawa, T. Nakamura, M. G. Mlynczak, and J. M. Russel III (2006), A multi-instrument measurement of a mesospheric front-like structure at the equator, *J. Meteorol. Soc. Jpn.*, *84A*, 305–316.

Smith, S. M., M. J. Taylor, G. R. Swenson, C.-Y. She, W. Hocking, J. Baumgardner, and M. Mendillo (2003), A multidiagnostic investigation of the mesospheric bore phenomenon, *J. Geophys. Res.*, *108*(A2), 1083, doi:10.1029/2002JA009500.

Smith, S. M., J. Friedman, S. Raizada, C. Tepley, J. Baumgardner, and M. Mendillo (2005), Evidence of mesospheric bore formation from a breaking gravity wave event: Simultaneous imaging and lidar measurements, *J. Atmos. Sol. Terr. Phys.*, *67*, 345–356.

Smith, S. M., J. Scheer, E. R. Reisin, J. Baumgardner, and M. Mendillo (2006), Characterization of exceptionally strong mesospheric wave events using all-sky and zenith airglow observations, *J. Geophys. Res.*, *111*, A09309, doi:10.1029/2005JA011197.

Stockwell, R. G., M. J. Taylor, K. Nielson, and M. J. Jarvis (2006), A novel joint space-wave number analysis of an unusual Antarctic gravity wave event, *Geophys. Res. Lett.*, *33*, L08805, doi:10.1029/2005GL025660.

Swenson, G. R., J. Qian, J. M. C. Plane, P. J. Espy, M. J. Taylor, D. N. Turnbull, and R. P. Lowe (1998), Dynamical and chemical aspects of the mesospheric Na ‘‘wall’’ event on October 9,1993 during the Airborne Lidar and Observations of Hawaiian Airglow (ALOHA) campaign, *J. Geophys. Res.*, *103*(D6), 6361–6380.

Taylor, M. J., D. N. Turnbull, and R. P. Lowe (1995), Spectrometric and imaging measurements of a spectacular gravity wave event observed during ALOHA-93 campaign, *Geophys. Res. Lett.*, *22*(20), 2849–2852.

Taylor, M. J., W. R. Pendleton Jr., S. Clark, H. Takahashi, D. Gobbi, and R. A. Goldberg (1997), Image measurements of short period gravity waves at equatorial latitudes, *J. Geophys. Res.*, *102*(D22), 26,283–26,299.

Walterscheid, R. L., J. H. Hecht, R. A. Vincent, I. M. Reid, J. Woithe, and M. P. Hickey (1999), Analysis and interpretation of airglow and radar observations of quasi-monochromatic gravity waves in the upper mesosphere and lower thermosphere over Adelaide, Australia (35°S, 138°E), *J. Atmos. Sol. Terr. Phys.*, *61*, 461–478.

K. Emperumal, S. Gurubaran, and V. L. Narayanan, Equatorial Geophysical Research Laboratory, Indian Institute of Geomagnetism, Krishnapuram, Tirunelveli 627 011, India. (gurubara@iigs.iigm.res.in)